

# Rarefied flow past Supersonic Vehicles with Different Nose Cones

Sekhar Chavala

A Thesis Submitted to  
Indian Institute of Technology Hyderabad  
In Partial Fulfillment of the Requirements for  
The Degree of Master of Technology



भारतीय प्रौद्योगिकी संस्थान हैदराबाद  
Indian Institute of Technology Hyderabad

Department of Mechanical and Aerospace Engineering

June 2016

## Declaration

I declare that this written submission represents my ideas in my own words, and where ideas or words of others have been included, I have adequately cited and referenced the original sources. I also declare that I have adhered to all principles of academic honesty and integrity and have not misrepresented or fabricated or falsified any idea/data/fact/source in my submission. I understand that any violation of the above will be a cause for disciplinary action by the Institute and can also evoke penal action from the sources that have thus not been properly cited, or from whom proper permission has not been taken when needed.

---

(Signature)

---

(Sekhar Chavala)

---

(Roll No.)

## Approval Sheet

This Thesis entitled Rarefied flow past Supersonic Vehicles with Different Nose Cones by Sekhar Chavala is approved for the degree of Master of Technology from IIT Hyderabad

---

(Dr. Raja Banerjee) Examiner  
Dept. of Mechanical and Aerospace Engineering  
IITH

---

(Dr. Harish Nagaraj Dixit) Examiner  
Dept. Mechanical and Aerospace Engineering  
IITH

---

(Dr. Nishanth Dongari) Adviser  
Dept. of Mechanical and Aerospace Engineering  
IITH

## Acknowledgements

I'm grateful to my instructor Dr. Nishanth Dongari for allowing me freedom to work and at the time to keep an eye to see that I don't get drifted from the main objective. His mentor ship was paramount in providing a well rounded experience consistent my long-term career goals. And simultaneously, he has been the source of motivation for all our friends. Thus, the work environment, I have got to work has been vibrant and energetic.

I would like to thank my friends Apurva Bhagat and Harshal Gijare for valuable suggestions and helping me throughout my thesis journey for maintaining an atmosphere of co-operation and friendship.

I would like to thank Mechanical and Aerospace Department of IITH and the entire IIT Hyderabad system for providing us an excellent computational facility to work upon.

# Dedication

I would like to dedicate to my brother Prakash

## Abstract

The current work examined the rarefied supersonic flow around the different types of nose cone shapes in high Knudsen numbers. The nose cone shapes involving Conical, Bi-conic, Parabolic, Spherical Blunt cone and Tangent ogive are considered in evaluating the numerical simulation. These cases have been investigated with the first order Maxwell slip and Smoluchowski jump boundary conditions for two different Knudsen numbers (Kn) 0.05 and 0.5 as rarefaction conditions are existed in the outer-atmosphere. These conditions are implemented into the *rhoCentralFoam* solver in the OpenFoam software. The purpose of the work is to obtain the flow field properties about all these leading nose cone shapes computationally and compare the results with CFD results. Also, aerodynamic forces had been derived. The drag and lift forces are compared among five nose cone shapes. The results obtained in the supersonic flow regime show that the parabolic and tangent ogive nose cone shapes have the low mean shear stress on the surface and the parabolic nose cone shape had minimum tip temperature. in addition , tangent ogive has minimum mean surface temperature. Further more, the spherically blunted cone has maximum mean pressure on solid surface and also maximum tip pressure. Parabolic and Bi-Conic have minimum tip pressure.

# Contents

Declaration . . . . .	ii
Approval Sheet . . . . .	iii
Acknowledgements . . . . .	iv
Abstract . . . . .	vi
<b>1 Introduction</b>	<b>7</b>
1.1 The Scope of current work . . . . .	7
1.2 Literature review . . . . .	7
<b>2 Governing Equations</b>	<b>9</b>
2.1 Introduction . . . . .	9
2.2 Finite Volume Method . . . . .	9
2.3 Partial Differential Equations . . . . .	9
<b>3 Numerical Simulations</b>	<b>11</b>
3.1 Turbulence modeling . . . . .	11
3.1.1 Spalart Allmaras Simulation . . . . .	11
3.2 The <i>rhoCentralFoam</i> . . . . .	13
3.2.1 Algorithm for <i>rhoCentralFoam</i> . . . . .	13
3.2.2 CFL criteria . . . . .	14
3.2.3 Rarefied flow and Knudsen number . . . . .	14
3.2.4 Sutherland's Viscosity model . . . . .	14
3.3 Boundary Conditions . . . . .	15
<b>4 Validations</b>	<b>17</b>
4.0.1 Case Description . . . . .	17
4.1 when $Kn=0.05$ . . . . .	18
4.1.1 Effect of Pressure and Velocity effects on Nose cone shapes . . . . .	19
4.2 Effect of Drag and Lift forces . . . . .	24
4.2.1 Aerodynamic Forces . . . . .	24
4.2.2 Drag effects on each nose cone shape . . . . .	24
4.2.3 Coefficient of Pressure . . . . .	25
4.3 Effect of Pressure, Temperature and Velocity on parabolic cone shape . . . . .	26
4.4 when $Kn=0.5$ . . . . .	27
4.4.1 Effect of Pressure and Velocity effects on Nose cone shapes . . . . .	27

4.4.2	Pressure Distribution Comparison on all nose once shapes . . . . .	33
4.4.3	Wall Shear Stress . . . . .	34
4.4.4	Temperature Variations on all nose cone shapes . . . . .	35
4.4.5	Velocity Variations on all nose cone shapes . . . . .	36
<b>5</b>	<b>Grid Independence</b>	<b>37</b>
5.1	Grid independence test on Conical and Bi-conical nose cone . . . . .	37
5.2	Time independence . . . . .	40
<b>6</b>	<b>Conclusion and Future work</b>	<b>41</b>
	<b>References</b>	<b>42</b>



# List of Tables

3.1 Coefficients for the Spalart-Allmaras model . . . . .	12
---	----

# List of Figures

4.1	Geometry of all nose cone shapes . . . . .	18
4.2	Pressure distribution (a) and velocity (b) comparison between solution of <i>rhoCentralFoam</i> with slip BC and CFD results on solid surface . . . . .	19
4.3	Pressure distribution (a) and velocity (b) contours parabolic nose cone . . . . .	19
4.4	Pressure distribution (a) and velocity (b) comparison between solution of <i>rhoCentralFoam</i> with slip BC and CFD results on solid surface . . . . .	20
4.5	Pressure distribution (a) and velocity (b) contours on Spherically blunted cones . . .	20
4.6	Pressure distribution (a) and velocity (b) comparison between solution of <i>rhoCentralFoam</i> with slip BC and CFD results on solid surface . . . . .	21
4.7	Pressure distribution (a) and velocity (b) contours on Tangent Ogive shape . . . . .	21
4.8	Pressure distribution (a) and velocity (b) comparison between solution of <i>rhoCentralFoam</i> with slip BC and CFD results on solid surface . . . . .	22
4.9	Pressure distribution (a) and velocity (b) comparison between solution of <i>rhoCentralFoam</i> with slip BC and CFD results on solid surface . . . . .	23
4.10	Pressure distribution (a) and velocity (b) contours on Conical shape . . . . .	23
4.11	Principal forces acting on flight/missile . . . . .	24
4.12	Pressure, Temperature and Velocity variations for different AOA on Parabolic nose cone solid surface . . . . .	26
4.13	Pressure distribution (a) comparison between solution of <i>rhoCentralFoam</i> with slip BC and CFD results on Parabolic shape solid surface . . . . .	27
4.14	Pressure distribution (a) and velocity (b) contours of parabolic nose cone . . . . .	28
4.15	Pressure distribution (a) and velocity (b) comparison between solution of <i>rhoCentralFoam</i> with slip BC and CFD results on Sp.Blunted shape solid surface . . . . .	29
4.16	Pressure distribution (a) and velocity (b) contours on Spherically blunted cones . . .	29
4.17	Pressure distribution (a) comparison between solution of <i>rhoCentralFoam</i> with slip BC and CFD results on Tangent ogive shape solid surface . . . . .	30
4.18	Pressure distribution (a) and velocity (b) contours on Tangent Ogive cone . . . . .	30
4.19	Pressure distribution (a) and velocity (b) comparison between solution of <i>rhoCentralFoam</i> with slip BC and CFD results on Bi-conical shape solid surface . . . . .	31
4.20	Pressure distribution (a) and velocity (b) contours on Bi-conical nose cone . . . . .	31
4.21	Pressure distribution (a) and velocity (b) comparison between solution of <i>rhoCentralFoam</i> with slip BC and CFD results on Conical shape solid surface . . . . .	32
4.22	Pressure distribution (a) and velocity (b) contours on Conical nose cone . . . . .	32
4.23	Variations in Pressure on various nose cone shapes at $Kn = 0.5$ . . . . .	33

4.24	Variations in Wall Shear on various nose cone shapes at $Kn = 0.5$ . . . . .	34
4.25	Variations in Wall Shear on various nose cone shapes at $Kn = 0.5$ . . . . .	35
4.26	Variations in Slip Velocity on various nose cone shapes at $Kn=0.5$ . . . . .	36
5.1	Variations in Pressure Coefficient on Conical nose cone . . . . .	38
5.2	Variations in Pressure on Conical nose cone . . . . .	38
5.3	Variations in Pressure Coefficient on Bi-Conical nose cone . . . . .	39
5.4	Variations in Pressure on Bi-Conical nose cone . . . . .	39
5.5	Variations in Pressure Coefficient on Conical nose cone . . . . .	40

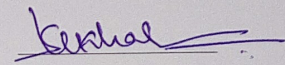
# List of Symbols

## *Nomenclature*

$C_h$	heat transfer coefficient
$C_p$	pressure coefficient
$C_D$	drag coefficient
$p$	pressure
$T$	temperature
$U$	velocity
$U_x$	axial velocity
$U_y$	radial velocity
$c_p$	specific heat at constant pressure
$H$	specific enthalpy
$k$	thermal conductivity
$R$	gas constant
$B$	Reynolds number
$Pr$	Prandtl number
$Kn$	Knudsen number
$Ma$	Mach number

## Declaration

I declare that this written submission represents my ideas in my own words, and where ideas or words of others have been included, I have adequately cited and referenced the original sources. I also declare that I have adhered to all principles of academic honesty and integrity and have not misrepresented or fabricated or falsified any idea/data/fact/source in my submission. I understand that any violation of the above will be a cause for disciplinary action by the Institute and can also evoke penal action from the sources that have thus not been properly cited, or from whom proper permission has not been taken when needed.



(Signature)

---

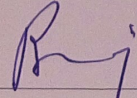
(Sekhar Chavala)

ME14MTECH11003

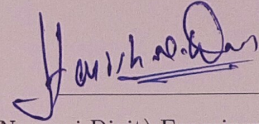
(Roll No.)

## Approval Sheet

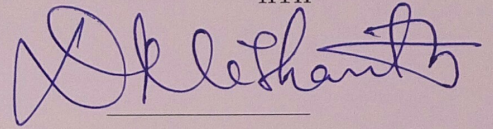
This Thesis entitled Rarefied flow past Supersonic Vehicles with Different Nose Cones by Sekhar Chavala is approved for the degree of Master of Technology from IIT Hyderabad



(Dr. Raja Banerjee) Examiner  
Dept. of Mechanical and Aerospace Engineering  
IITH



(Dr. Harish Nagaraj Dixit) Examiner  
Dept. Mechanical and Aerospace Engineering  
IITH



(Dr. Nishanth Dongari) Adviser  
Dept. of Mechanical and Aerospace Engineering  
IITH

13/07/2016

# Chapter 1

## Introduction

### 1.1 The Scope of current work

One of the main design factors that affect projectile of rockets, missiles and bullets is nose cone. Nose cones may have many varieties of shapes, most common of which are conical, ogival, power series or hemispherical. The shape of the nose cone must be chosen for minimum drag and hence a solid of revolution is used that gives least resistance to motion. A nose cone can have many shapes which are used primarily on the missiles traveling at supersonic speeds and are generally selected on the basis of combined aerodynamic, guidance and structural considerations. The aerodynamic design of the nose cone section of any vehicle or body meant to travel through a compressible fluid medium (such as a rocket or aircraft, missile or bullet), an important problem is the determination of the nose cone geometrical shape for optimum performance. For many applications, such a task requires the definition of a solid of revolution shape that experiences minimal resistance to rapid motion through such a fluid medium, which consists of elastic particles.

The accurate simulation of non-equilibrium rarefied gas flows remain very challenging in the field of computational fluid dynamics (CFD) in the design, analysis, and optimization of flight systems. The nose of the supersonic missiles especially at high Mach number plays important role in performance of missile and possibility of severe heating effects beyond the speed of sound speed (Hypersonic). Therefore a study of aerodynamic of nose shapes in supersonic missiles is required for increasing the speed upto desired Mach number. Computational simulations of non-equilibrium rarefied gas flows requires knowledge of the kinetic theory of gases and understanding of different numerical simulations method such as CFD, Direct Simulation Monte-Carlo (DSMC).

The design of re-entry or air vehicles requires accurate prediction of the surface properties in flight such as surface temperature, pressure, heat transfer and shear stress.

### 1.2 Literature review

The accurate simulation of non-equilibrium rarefied gas flows remain very challenging in the field of computational fluid dynamics (CFD) in the design, analysis, and optimization of flight systems [1, 2]. The nose of the supersonic missiles especially at high Mach number plays important role in performance of missile and possibility of severe heating effects [3] beyond the speed of sound speed

(Hypersonic). Therefore a study of aerodynamic of nose shapes in supersonic missiles is required for increasing the speed upto desired Mach number. The design of re-entry or air vehicles requires accurate prediction of the surface properties in flight such as surface temperature, pressure, heat transfer and shear stress.

Previous work found that there was a significant difference between the N-S-F and experimental density fields [4, 5]. Wang and Bao investigated the Aerothermodynamics of hypersonic small nose cone with local rarefied gas effects [6]. Markus Gauer numerically investigated on spike blunted nose cones at Hypersonic flow [7]. The Bi-conic case has been carefully simulated by many researchers. Recently Graham V. Candler and Ioannis Nompelis have investigated on Bi-conic nose cone shape at high enthalpy [8]. Then, E. Titov, J. Burt, E. Josyula, I. Nompelis have implemented the slip boundary conditions to find the surface flow field properties [9].

Stephen C. Traugott have numerically have obtained Pressure distributions about blunted cones in Supersonic and Hypersonic flows from the Belotserkovskii Method and also done experimentally, and these results are used to study convergence to conical flow [10]. Owens and Robert V have experimentally investigated on Spherically blunted cones at Mach number 0.5 to 5.0 [11]. Burke, G. L. studied on Pressure distribution and Heat transfer over sharp and blunted elliptic cones at different angle of attacks and Mach numbers [12]. Wilson F.N. Santos and Mark Lewis have numerically investigated on the Power Law blunted shaped leading edges situated in rarefied hypersonic flow by using Direct Simulation Monte Carlo (DSMC) Method [13]

P.A.Newman and J.C. South had used The method of integral relations to calculate supersonic flow past ogive shaped bodies and Pressure distributions and shock-wave curvature at the tip of ogive bodies [14].



# Chapter 2

## Governing Equations

### 2.1 Introduction

In this chapter we discuss the Governing equations and their partial differential forms. The discretization is carried out in Finite Volume Method (FVM).

### 2.2 Finite Volume Method

The Finite volume method utilizes an integration over a control volume. The control volume is constructed from a given mesh. Depending on whether the mesh is unstructured or structured the control volumes for every cell node is created differently. The Gaussian theorem is used to simplify terms in the governing equations,

$$\int_{CV} \frac{\partial \phi_i}{\partial x_i} dV = \int_A n_i \phi_i dA_i \quad (2.1)$$

where,

$CV$  = Control Volume

$A$  = Area of the control volume

$n_i$  = normal vector to the surface integral.

### 2.3 Partial Differential Equations

Navier-Stokes-Fourier equations can be represented as following.

Continuity Equation (Conservation of mass)

$$\frac{\partial \rho}{\partial t} + \nabla \cdot (\rho V) = 0 \quad (2.2)$$

Conservation of momentum with neglecting gravity

$$\frac{\partial(\rho V)}{\partial t} + \nabla \cdot [V(\rho V)] + \nabla p + \nabla \cdot \sigma = 0 \quad (2.3)$$

where  $\sigma$  is viscous stress tensor and positive in compression

Conservation of Energy

$$\frac{\partial(\rho E)}{\partial t} + \nabla \cdot [V(\rho E)] + \nabla \cdot (Vp) + \nabla \cdot (\sigma \cdot V) = \nabla \cdot (k \nabla T) \quad (2.4)$$

where,  $(\rho E)$  is total energy of the system;  $k$  is thermal conductivity; and  $T$  is Temperature and  $E = e + \frac{1}{2}|u^2|$ , where  $e = c_v T = (\gamma - 1)RT$  is specific internal energy and  $\gamma = \frac{c_p}{c_v}$  is the ratio of specific heats at constant pressure and volume, where  $p = \rho RT$  and  $R$  is gas constant. The value of temperature is calculated as,

$$T = \frac{1}{c_v} \left( \frac{\rho E}{\rho} - \frac{|u|^2}{2} \right) \quad (2.5)$$

## Chapter 3

# Numerical Simulations

The Navier-Stokes-Fourier (N-S-F) equations are implemented and solved numerically with the high-resolution central scheme in OpenFOAM as the solver *rhoCentralFoam*. OpenFOAM [15] is an open source software developed by OpenCFD Ltd. for computational fluid dynamic simulations with many different solvers. There are four solvers for single phased highly compressible fluids and one multiphase solver for slightly and semi-compressible fluids. OpenFOAM is first and foremost a C++ library, used primarily to create executables, known as applications. New solvers and utilities can be created by its users with some pre-requisite knowledge of the underlying method, physics and programming techniques involved.

### 3.1 Turbulence modeling

The prediction of the flow phenomena such as boundary layer separation or shock interactions depends on the turbulence model. Turbulence is ubiquitous phenomenon. Fluid flows generally encountered in engineering applications are turbulent in nature which is characterized by

1. Random and Chaotic nature - temporally and spatially.
2. Diffusivity - intense mixing due to the fluctuating quantities.
3. Large Reynolds number phenomenon - occurs at high Re number regime.
4. Three-Dimensionality 1 - fluctuations are three dimensional even though the mean flow field is two dimensional.
5. Rotationality - always involves vortices.
6. Dissipative - more energy consuming compared to laminar flow.
7. Continuum - smallest possible eddies in the flow field are larger than the molecular mean free path

#### 3.1.1 Spalart Allmaras Simulation

Several one-equation transport models for turbulence have appeared over the years. The most popular one-equation models have been the Baldwin-Barth model [16] and the Spalart-Allmaras model [17]

We have used Spalart Allmaras [17] one equation turbulence modeling. One equation model such as the Spalart Allmaras model provides a compromise between algebraic and two equation models.

The Spalart Allmaras one equation model solves directly a transport equation for the eddy viscosity, became popular because of its reasonable results for a wide range of flow problems and its numerical properties.

The Spalart-Allmaras turbulence model was derived using empirical relationships, dimensional analysis, and Galilean invariance. The goal was to produce a turbulent transport model that was fast, numerically stable, and reasonably accurate for both shear layers and boundary layers. The model uses a turbulence variable  $\bar{\nu}$  that has the dimensions of viscosity. The model can be written as

$$\frac{\partial \bar{\nu}}{\partial t} + U_i \frac{\partial \bar{\nu}}{\partial x_i} = \frac{1}{\sigma} [\nabla \cdot ((\nu + \bar{\nu}) \nabla \bar{\nu}) + C_{b_2} (\nabla \bar{\nu})^2] + P(\bar{\nu}) - D(\bar{\nu}) \quad (3.1)$$

where the production term is given by

$$P(\bar{\nu}) = C_{b_1} \bar{\nu} [\Omega + \frac{\bar{\nu}}{k^2 d^2} f_{v_2}] \quad (3.2)$$

The production function for turbulence models are usually functions of the eddy viscosity and the fluid strain or vorticity.

and the dissipation is given by

$$D(\bar{\nu}) = C_{w_1} f_w \left[ \frac{\bar{\nu}}{d} \right]^2 \quad (3.3)$$

Here  $\Omega$  is the magnitude of the vorticity,  $d$  is the distance to the nearest wall, and  $f_{v_2}$  and  $f_w$  are given by

$$f_{v_2} = 1 - \left[ \frac{\alpha}{1 + \alpha f_{v_1}} \right] \quad (3.4)$$

$$f_w = g \left[ \frac{1 + C_{w_3}^6}{g^6 + C_{w_3}^6} \right]^{\frac{1}{6}} \quad (3.5)$$

and the remaining functions are given by

$$f_{v_1} = \frac{\alpha^3}{\alpha^3 + C_{v_1}^3} \quad (3.6)$$

$$\alpha = \frac{\bar{\nu}}{\nu} \quad (3.7)$$

$$g = r + C_{w_2} (r^6 - r) \quad (3.8)$$

$$r = \frac{\bar{\nu}}{\Omega k^2 d^2 + \bar{\nu} f_{v_2}} \quad (3.9)$$

The remaining constants are given in Table below

Table 3.1: Coefficients for the Spalart-Allmaras model

$C_{b_1}$	$C_{b_2}$	$\sigma$	$k$	$C_{w_1}$	$C_{w_2}$	$C_{v_1}$
0.1355	0.622	2/3	0.41	$C_{b_1}/k + \frac{1+C_{b_2}}{\sigma}$	0.3	7.1

The Spalart-Allmaras turbulence model is a very stable and generally reasonably accurate model for a wide range of turbulent flows. The model is relatively easy to implement in both structured and unstructured Navier-Stokes codes. One drawback is the model requires the calculation of the distance to the nearest wall for all field points. This can be an expensive computation, especially

for unstructured grid codes. The model has been used extensively for threedimensional geometries and is well documented. The model has been used with some success for some unsteady flows.

## 3.2 The *rhoCentralFoam*

The *rhoCentralFoam* is the density-based compressible flow solver based on central-upwind schemes of Kurganov and Tadmor [18, 19]. Christopher *et al* [20] has provided details of this solver and validation against standard high viscous flow test cases. Various compressible solvers had been compared in literature against the *rhoCentralFoam*, given better predictive capabilities for high speed flows.

### 3.2.1 Algorithm for *rhoCentralFoam*

This solver is solving each of the governing compressible equations separately. First the continuity equation is solved, providing a new value for  $\rho$ . Thereafter the momentum equation is solved in two steps where first the inviscid part is calculated explicitly for a predicted a variable value and the values updated and afterwards the viscid part is added by time splitting method. The energy equation is first solved without the diffusive flux of heat, which is later added when the updated temperature is calculated. The predicted velocity value is determined explicitly from the momentum equation like below:

$$\frac{(\rho\bar{u}) - (\rho u)^{n+1}}{\partial t} + \nabla \cdot u[u(\rho u)] + \nabla p = 0 \quad (3.10)$$

$$\bar{u} = \frac{\rho\bar{u}}{\rho} \quad (3.11)$$

To determine the corrected velocity value implicitly at the next time step (n+1), this predicted value is used by the viscous momentum equation below:

$$\frac{(\rho u)^{n+1} - (\rho u)}{\partial t} - \nabla \cdot (\mu \nabla u) = 0 \quad (3.12)$$

The solution of the energy equation follows the similar procedure.  $(\rho E)$  the energy predictive value is calculated from the inviscid energy equation:

$$\frac{\partial(\rho E)}{\partial t} + \nabla \cdot [u(\rho E)] + \nabla \cdot (T \cdot u) = 0 \quad (3.13)$$

The temperature T is determined and considering the parameter  $\rho$ ,  $u$  and  $E$  which is used to corrected energy equation:

$$\frac{\partial(\rho C_v T)}{\partial t} + \nabla \cdot (K \nabla T) = 0 \quad (3.14)$$

Then the pressure is updated by the equation of state for the ideal gas. To determine the viscosity Sutherlands law of viscosity is used.

This solver has been validated with supersonic compressible flow around circular cylinder and backward-facing step. The flow fields are computed by the steady Reynolds-Averaged Navier-Stokes (RANS) solver with Spalart Allmaras one-equation turbulence model.

### 3.2.2 CFL criteria

*rhoCentralFoam* solver is an explicit solver, we will have time stepping criteria. The Courant-Friedrich-Lewy condition is a numerical constraint which determines the allowed time step for a specific grid size. This constraint determines that information can only propagate no further than one cell away from the original cell. In explicit schemes this constraint is necessary for convergence. If information propagates with the speed  $u$ , then the CFL number is given in equation for a one dimensional case

$$u \frac{\Delta t}{\Delta x} < C \quad (3.15)$$

where,

$\Delta t$  is time step,

$\Delta x$  is grid size,

and  $C$  is a number which determines the CFL condition.

For explicit schemes  $C < 1$  and for implicit schemes it can be larger [21].

### 3.2.3 Rarefied flow and Knudsen number

Rarefied gas dynamics is based on the kinetic approach to gas flows. Maxwell [22] gave the origin to the kinetic theory of gases. Then, Boltzmann deduced the kinetic equation which determines the evolution of the distribution function for gaseous systems being out of equilibrium. The principal parameter of rarefied gas dynamics is the Knudsen number ( $Kn$ ) which characterizes the gas rarefaction and is defined as the ratio,

$$Kn = \frac{\lambda}{L} \quad (3.16)$$

where,

$\lambda$  is the mean free path,

$L$  is characteristic length of the geometry. The magnitude of the Knudsen number determines the appropriate gas dynamic regime. When the Knudsen number is small compare to unity, if the order of  $Kn < 0.001$ , the fluid can be treated as continuum regime, the N-S-F equation with standard no-slip boundary condition can be employed to describe the flow behavior. In slip regime,  $0.001 < Kn < 0.1$ , the N-S-F equations should be accompanied with the velocity slip and temperature jump boundary conditions over the walls. In the transition regime,  $0.1 < Kn < 10$ , the core flow gradually departs from the equilibrium and the N-S-F equations are no longer valid. Finally, the flow considered as free molecular as it goes beyond the limit of  $Kn > 10$ .

### 3.2.4 Sutherland's Viscosity model

Sutherland's formula for viscosity gives a relationship between the temperature  $T$  and the dynamic viscosity of fluid [23]. It is based on the kinetic theory of gases ( Kinetic Theory ). But it is still commonly used and gives fairly accurate results.

It is expressed as:

$$\mu = \mu_{ref} * \left( \frac{T_{ref} + C}{T + C} \right) * \left( \frac{T}{T_{ref}} \right)^{1.5} \quad (3.17)$$

where

$\mu$ = dynamic viscosity (Pa.s) at input temperature  $T$   
 $\mu_{ref}$ = reference viscosity (Pa.s) at reference temperature  $T_{ref}$   
 $T$ = input temperature ( $K$ )  
 $T_{ref}$  = reference temperature ( $K$ )  
 $C$ = Sutherland's constant for the gaseous material.

Valid for temperatures between  $0 < T < 555 K$  with the error due to pressure less than 10 % below 3.45 MPa.  $T = 110.4 K$  is the reference temperature.  $\mu_{ref} = 1.716 \times 10^{-5} \frac{N.s}{m^2}$  is the reference viscosity.

### 3.3 Boundary Conditions

The continuum regime of gas flows are simulated by solving Navier-Stokes-Fourier (N-S-F) equations with no-slip velocity boundary condition and no temperature jump boundary conditions. However in the rarefied flow region the experiments such as performed by Arkilic[24] and Colin[25] shown that the conventional N-S-F equations may not give accurate results. It is normal practice to determine the rarefaction degree of gas flows by the Knudsen number ( $Kn$ ). The N-S-F equations applied with continuous boundary conditions of velocity and temperature are commonly known to be valid up to a Knudsen number of 0.001 if no discontinuous boundary conditions are applied[26]. But in non-equilibrium boundary conditions for Knudsen number  $Kn \sim 0.1$ , slip velocity boundary conditions and temperature jump conditions are applied[27].

The first order Maxwell slip boundary condition can be expressed as,

$$U_f - U_w = \frac{2 - \sigma_v}{\sigma_v} \lambda \frac{\partial u}{\partial y} + \frac{3}{4} \frac{\mu}{\rho T} \frac{\partial T}{\partial x} \quad (3.18)$$

where,

$U_f$  is the fluid velocity,

$U_w$  is the reference wall velocity,

$\lambda$  is the mean free path of gas,

$\mu$  is the dynamic viscosity,

$\rho$  is the density of fluid,

$x$  is the axial co-ordinate,

$y$  is the normal co-ordinate,

$\sigma_v$  is tangential momentum accommodation coefficient

$T$  is the temperature.

The Smoluchowski temperature jump boundary condition can be written as,

$$T_f - T_w = \frac{2 - \sigma_T}{\sigma_T} \frac{2\gamma}{\gamma + 1} \frac{\lambda}{Pr} \frac{\partial T}{\partial y}, \quad (3.19)$$

and,  $Pr$  is non-dimensional Prandtl number, can be defined by

$$Pr = \frac{\mu C_p}{k}, \quad (3.20)$$

where,

$T_f$  is the fluid temperature,

$T_w$  is the reference wall temperature,  
 $\sigma_T$  is thermal accommodation coefficient,  
 $\gamma$  is specific heat ratio,  
 $C_p$  is specific heat,  
 $k$  is thermal conductivity.



# Chapter 4

## Validations

We have examined the flow field properties around conical, Bi-conic, parabolic, spherical Blunt and tangent ogive nose cones. The geometry of these bodies is shown in Figure ?? . The length of forebody is 0.3 m. The diameter and length of aftbody circular cylinder are 0.2 m and 1.5 m, respectively. The simulations are done for two Knudsen numbers(Kn=0.05,0.5) with air. Computational domain is a 2 dimensional cone shapes which is considered symmetric about axis. Mesh has been created with ICEM CFD tool with unstructured grids. The same Mesh of all nose cone shapes is used to obtain results using compressible solver *rhoCentralFoam* of OpenFOAM and compared with CFD results. In the first case for the selected Knudsen number (Kn=0.05), both the tangential momentum and the energy accommodation coefficient are selected equal to 0.85. The incident Mach number, ambient temperature and wall temperature are considered M=5, T=250 K, T=500 K, respectively. The pressure at the far field boundaries will be calculated from the following equation:

$$n = \frac{1}{\sqrt{2\pi}d^2 LKn} \quad (4.1)$$

where,  $p = nkT$

p=pressure (pa)

n=number density

k=Boltzmann constant

Kn=Knudsen number

L=Characteristic length of the flow field

d=Molecular diameter

### 4.0.1 Case Description

To solve all fluid properties such as pressure, temperature, velocity, a fully unstructured mesh of the geometry using ICEM CFD will be created first to solve all fluid properties such as pressure, temperature, velocity by using the *rhoCentralFoam*. The Geometry that has used for investigation is 2 Dimensional and shown in Figure 4.0.1

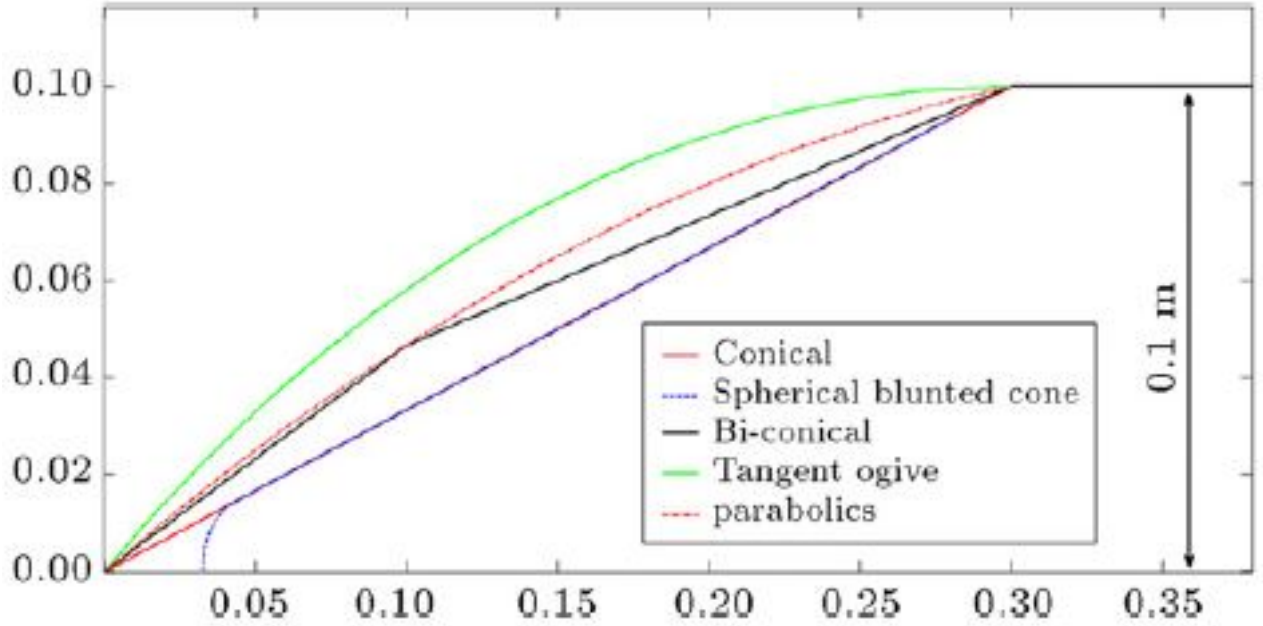


Figure 4.1: Geometry of all nose cone shapes

#### 4.1 when $Kn=0.05$

The flow regime can be defined by Knudsen number. There are four flow regimes.

1. Continuum regime for  $Kn < 0.01$
2. Slip-flow regime for  $0.01 < Kn < 0.1$
3. Transition flow regime for  $0.1 < Kn < 10$
4. Free-molecular flow regime for  $Kn > 10$ .

In this case the Knudsen number is 0.05 have been used to calculate the flow parameters such as Pressure, Temperature, Velocity, Shear Stress and Pressure coefficient. As we mentioned above the flow is slip-flow regime. In slip flow regime first order slip boundary conditions are applicable. Maxwell slip-velocity boundary conditions and Smoluchowski temperature jump boundary conditions over wall are used.

We have numerically investigated flow field parameters around all nose cone shapes such Conical, bi-conic, Parabolic, Spherically blunted cone and Tangent ogive with Knudsen numbers( $Kn$ ) 0.05 and compared with CFD results. The Pressure contours are in the excellent agreement but the velocity contours illustrate some differences.

### 4.1.1 Effect of Pressure and Velocity effects on Nose cone shapes

#### Parabolic nose cone

For the selected Knudsen number ( $Kn=0.05$ ) we have applied Maxwell's velocity slip and Smoluchowski temperature jump boundary conditioned.

The below Figure 4.2 shows the pressure and velocity variation on parabolic nose cone surface.

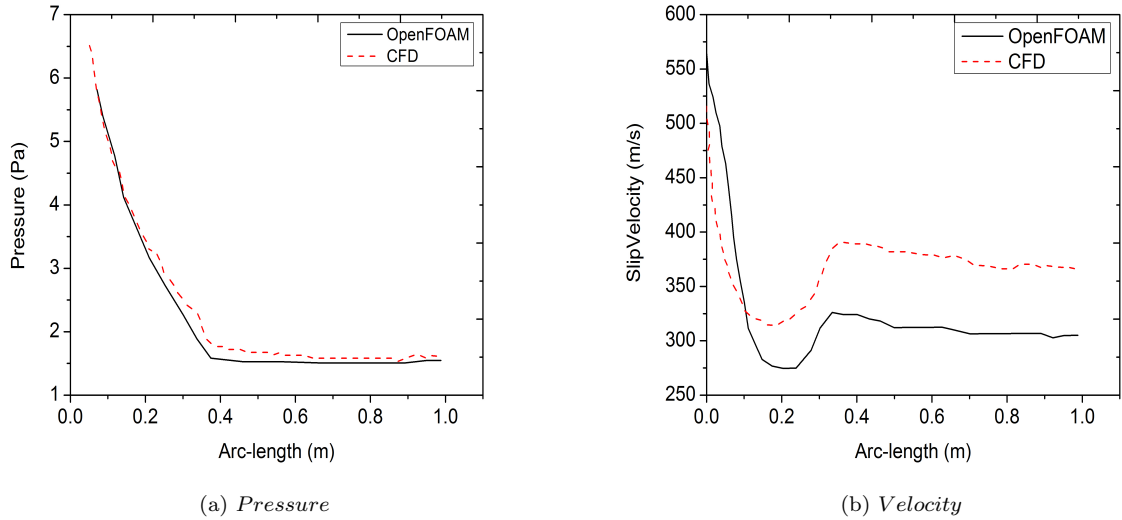


Figure 4.2: Pressure distribution (a) and velocity (b) comparison between solution of *rhoCentralFoam* with slip BC and CFD results on solid surface

The below Figure 4.3 shows the pressure and velocity contours on the parabolic nose cone.

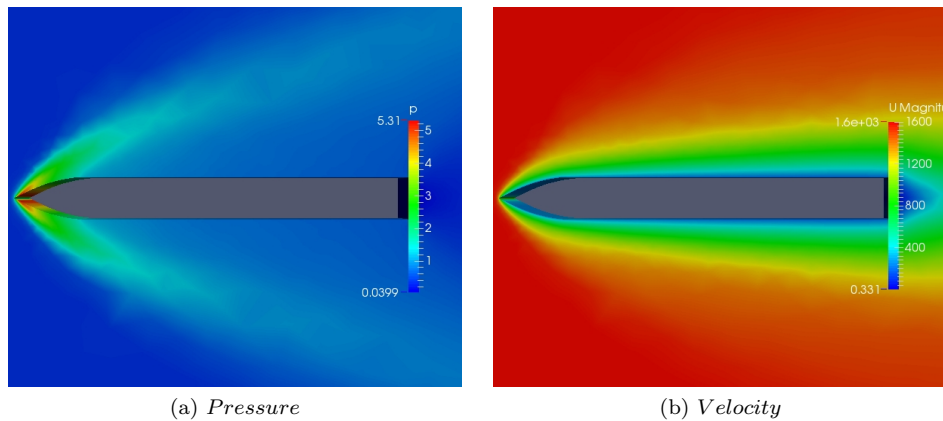


Figure 4.3: Pressure distribution (a) and velocity (b) contours parabolic nose cone

The mean pressure of the solid surface is 1.412 Pa which is lowest pressure among all the nose cone shapes. The mean velocity is of 210.9 m/s which is higher among all cone shapes.

### Spherically blunted nose cone

For the selected Knudsen number  $Kn=0.05$  as it is slip-flow regime, we have applied Maxwell's velocity slip and Smoluchowski temperature jump boundary conditions.

The below Figure 4.4 shows the Pressure distribution and Velocity variations on Spherically Blunted nose cone.

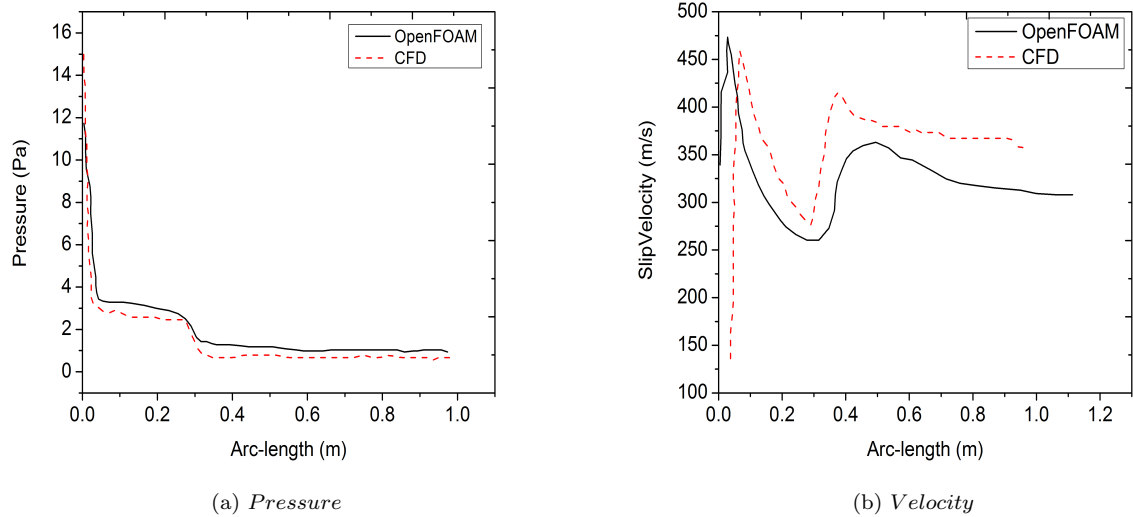


Figure 4.4: Pressure distribution (a) and velocity (b) comparison between solution of *rhoCentralFoam* with slip BC and CFD results on solid surface

The below Figure 4.5 shows the Pressure and Velocity contours.

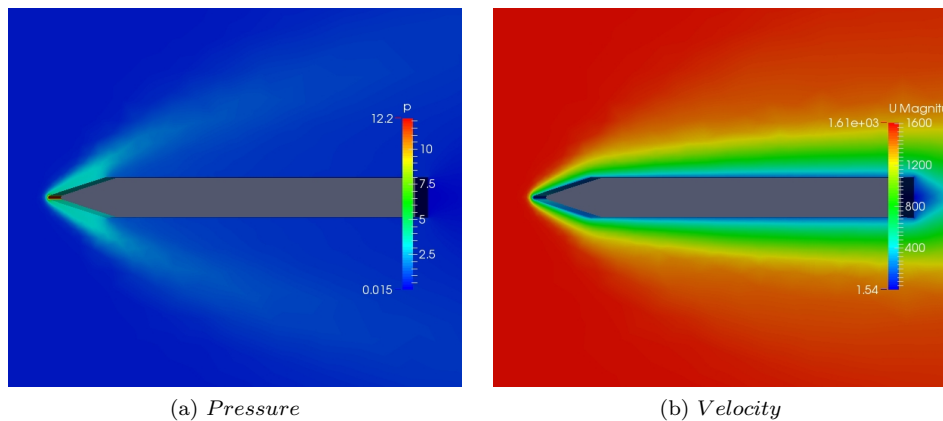


Figure 4.5: Pressure distribution (a) and velocity (b) contours on Spherically blunted cones

The mean pressure on the solid surface is 1.99 Pa which the maximum mean Pressure in all and also, from the plots spherically blunted nose cone has maximum tip pressure.

### Tangent ogive nose cone

For the selected Knudsen number ( $Kn=0.05$ ), slip-flow regime so that we have applied Maxwell's velocity slip and Smoluchowski temperature jump boundary conditions.

The below Figure 4.6 shows the pressure distribution and Velocity on the solid surface of Tangent Ogive shape.

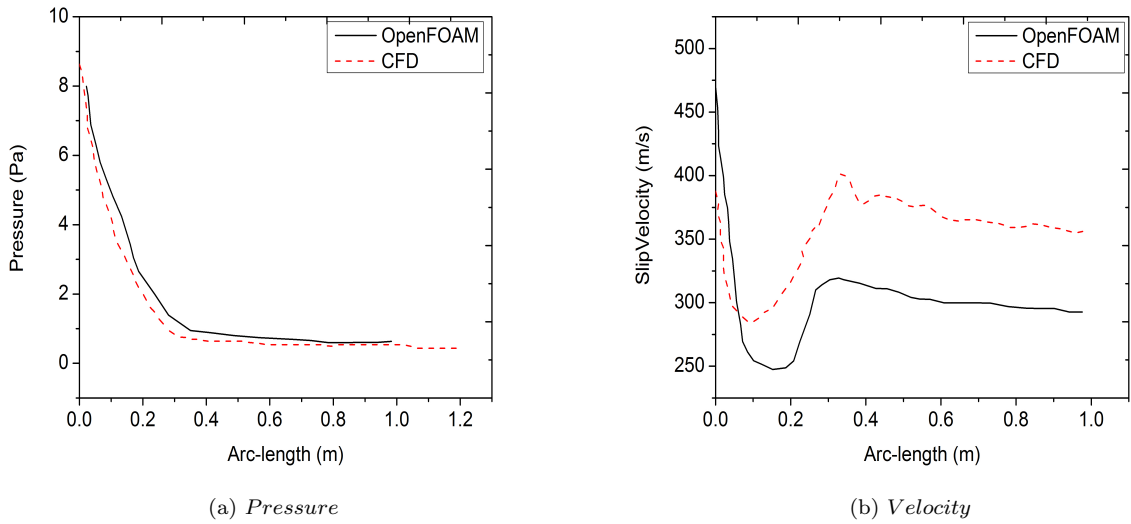


Figure 4.6: Pressure distribution (a) and velocity (b) comparison between solution of *rhoCentralFoam* with slip BC and CFD results on solid surface

The below Figure 4.7 shows the pressure and velocity contours.

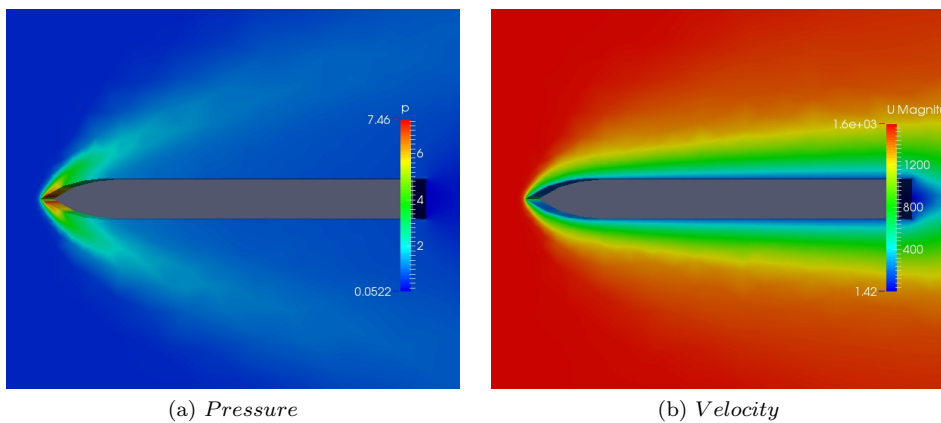


Figure 4.7: Pressure distribution (a) and velocity (b) contours on Tangent Ogive shape

The mean Pressure distribution on Tangent Ogive solid nose cone surface is 1.96 Pa and the mean velocity on the solid surface is 195.33 m/s.

### Biconical nose cone

For the selected Knudsen number ( $Kn=0.05$ ) we have applied Maxwell's velocity slip and Smoluchowski temperature jump boundary conditions.

The below Figure 4.8 shows the Pressure distribution and velocity on the solid surface of Biconical nose cone shape.

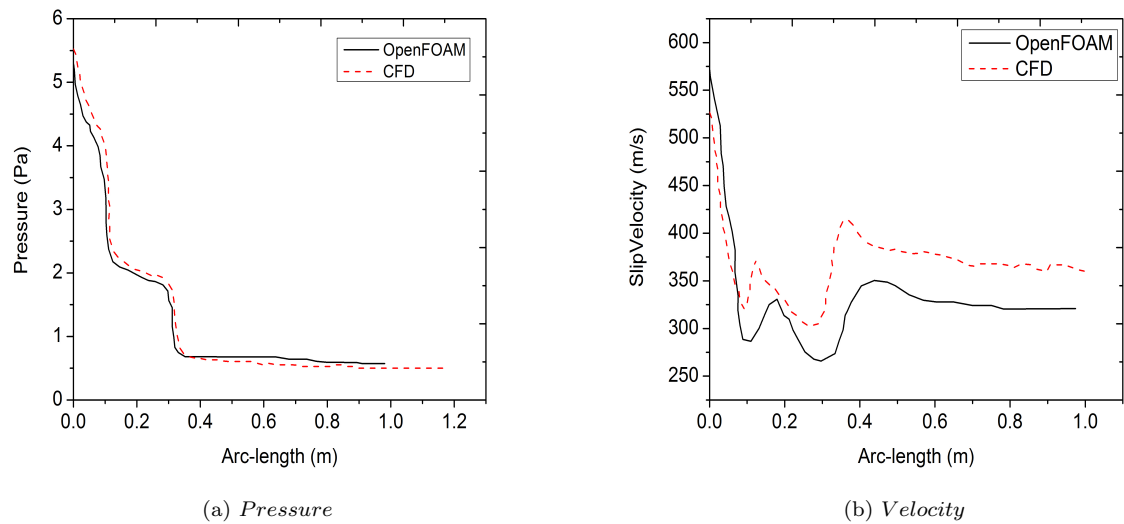


Figure 4.8: Pressure distribution (a) and velocity (b) comparison between solution of *rhoCentralFoam* with slip BC and CFD results on solid surface

The minimum tip Pressure distribution is of 1.53Pa which is almost equal to parabolic shape. The mean velocity on the solid surface is 205.3 m/s.

### Conical nose cone

For the selected Knudsen number ( $Kn=0.05$ ) we have applied Maxwell's velocity slip and Smoluchowski temperature jump boundary conditions.

The below 4.9 shows the pressure distribution and velocity on the Conical solid nose cone shape.

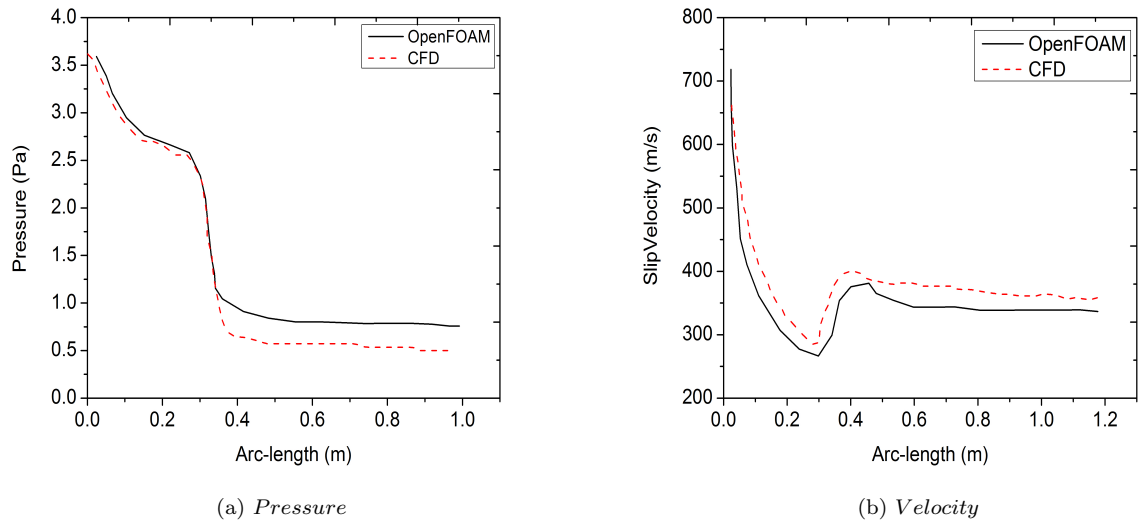


Figure 4.9: Pressure distribution (a) and velocity (b) comparison between solution of *rhoCentralFoam* with slip BC and CFD results on solid surface

The below Figure 4.10 shows the pressure and velocity contours.

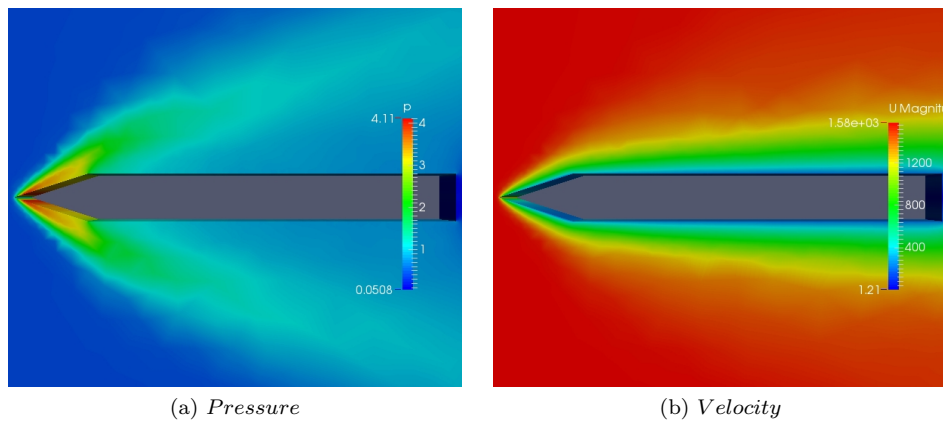


Figure 4.10: Pressure distribution (a) and velocity (b) contours on Conical shape

## 4.2 Effect of Drag and Lift forces

### 4.2.1 Aerodynamic Forces

The principal forces acting on a missile in level flight are thrust, drag, weight, and lift. Like any forces, each of these is a vector quantity.

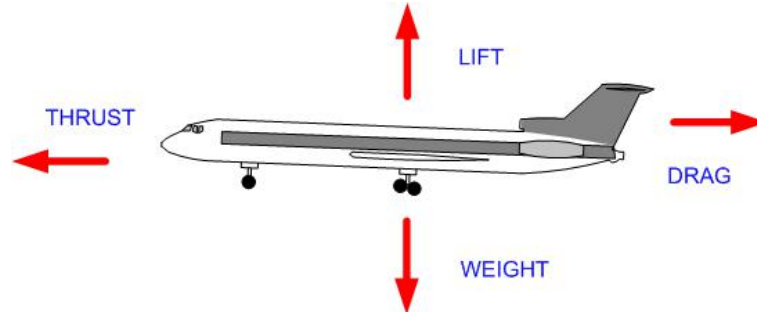


Figure 4.11: Principal forces acting on flight/missile

**Thrust** force is directed along the longitudinal axis of the missile and is the force which propels it forward at speeds sufficient to sustain flight.

**Drag** is the resistance air offers to the passage of the missile through air, and is directed rearward. Drag is a horizontal force acting to the flight/missile path and is opposed to thrust

**Gravity/Weight** of the missile is the pull of gravity on the missile, and is directed downward toward the center of the earth.

**Lift** is opposed to the force of gravity. The Lift force is perpendicular direction to the Drag force' direction.

### 4.2.2 Drag effects on each nose cone shape

Drag is an unavoidable consequence of an object moving through a fluid. Drag is the force generated parallel and in opposition to the direction of travel for an object moving through a fluid. Drag can be broken down into the following two components:

1. Form drag (or pressure drag) - dependent on the shape of an object moving through a fluid.
2. Skin friction - dependent on the viscous friction between a moving surface and a fluid, derived from the wall shear stress.

The shape of the nose cone must be chosen for minimum drag and hence a solid revolution is used that gives least resistance to motion. Given the problem of the aerodynamic design of the nose cone section of any vehicle or body meant to travel though a compressible medium (such as rocket or aircraft, missile or bullet), an important problem is the determination of the nose cone geometrical shape for optimum performance. For many applications, such as a task requires the definition of a solid of revolution shape that experiences minimal resistance to rapid motion through such a fluid medium, which consists of elastic particles.

The drag force acting on a body in fluid flow can be expressed as

$$F_D = C_D * \frac{1}{2} * \rho * V^2 * A \quad (4.2)$$



where

$F_D$  = drag force(N)

$C_D$  = drag coefficient

$\rho$  = density of fluid ( $kg/m^3$ )

$V$  = flow velocity ( $m/s$ )

$A$  = body area ( $m^2$ )

The drag force have been investigated at different angle of attacks such as 4, 10, 16 and 20. The below plots shown the variations of drag force on the solid surfaces of each nose cone shapes at different angle of attacks.

Increasing angle of attack is associated with increasing drag coefficient up to the maximum drag coefficient, at small angle of attacks the drag force is nearly constant. When the boundary layer separates, the wing is said to be stalled (Critical angle f attack) and both drag and lift become unsteady. Determining the drag is very difficult under stalled conditions. At and beyond the critical angle, drag increases enormously and lift drops to nearly zero.

### 4.2.3 Coefficient of Pressure

The pressure coefficient is a dimensionless number which describes the relative pressures throughout a flow field in fluid dynamics. The pressure coefficient is used in aerodynamics and hydrodynamics. Every point in a fluid flow field has its own unique pressure coefficient,  $C_p$ . In many situations in aerodynamics and hydrodynamics, the pressure coefficient at a point near a body is independent of body size.

The Pressure coefficient  $C_p$  shows the dynamic relative pressure on the critical wall, which is defined as below

$$C_p = \frac{p - p_\infty}{\frac{1}{2}\rho_\infty U_\infty^2} \quad (4.3)$$

Where

$p$  = Static Pressure on the critical wall,

$\rho_\infty$  = Freestream density,

$U_\infty$  = Freestream Velocity,

$U_\infty$  is calculated from chamber conditions. We define it as

$$U_\infty = \sqrt{\gamma RT_0} \quad (4.4)$$

Where

$\gamma$  = Specific heat ratio

$R$  = Gas constant for air

$T_0$  = Stagnation temperature

### 4.3 Effect of Pressure, Temperature and Velocity on parabolic cone shape

The below Figure 4.12 shows how the Pressure, Temperature and Velocity varies for different angle of attacks on the parabolic nose cone solid surface.

The below Figure 4.12 shows the Pressure, Temperature and Velocity on the Parabolic nose cone at different angle of attacks such as 4, 10, 16, 20.

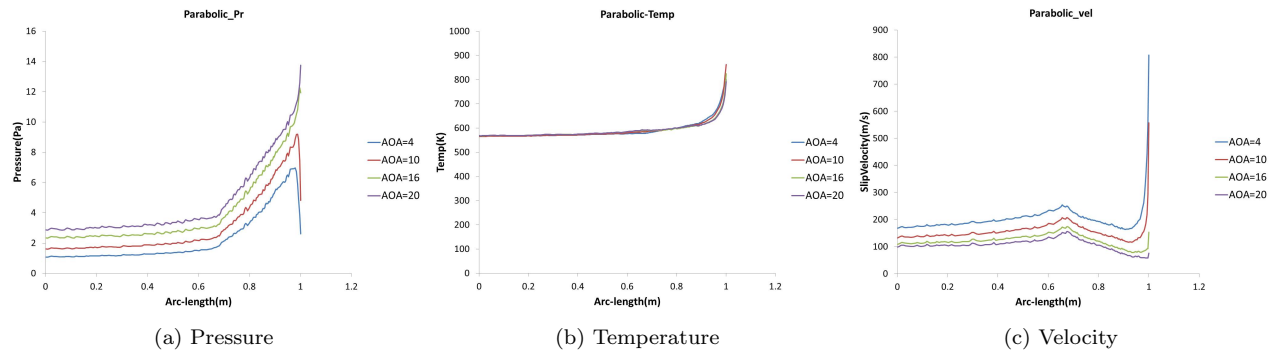


Figure 4.12: Pressure, Temperature and Velocity variations for different AOA on Parabolic nose cone solid surface

In the Pressure plot, as the angle of attack increase the pressure on the surface increases. In the Temperature plot, all the temperatures for all angle of attacks such as 4, 10, 16, 20 are almost similar. In the Velocity plot, as the angle of attack increase the velocity on the surface decreases.

## 4.4 when $Kn=0.5$

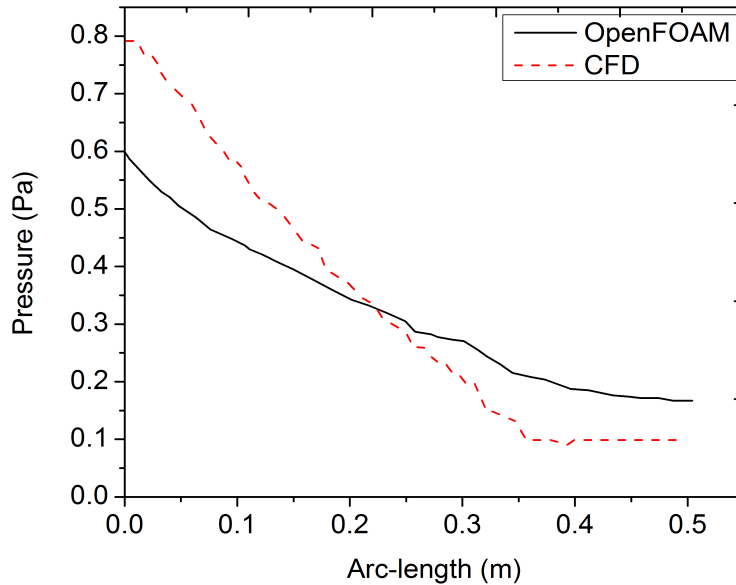
The flow regimes are defined based on the Knudsen number. For  $0.01 < Kn < 0.1$  the flow is called to be slip flow, for  $0.1 < Kn < 10$  then the flow is called as Transition flow, and for  $Kn > 10$  then the flow is called free-molecular flow. The transition flow is the most difficult to treat, is the subject of the present study. In transition regime (according to the literature present) higher order slip boundary conditions may be valid. Transition regime with high Knudsen number and free molecular regime need molecular dynamics.

### 4.4.1 Effect of Pressure and Velocity effects on Nose cone shapes

#### Parabolic nose cone

For the selected Knudsen number ( $Kn=0.5$ ) we have applied Maxwell's velocity slip and Smoluchowski temperature jump boundary conditioned. In this case for  $Kn = 0.5$ , the wall surface is considered to be adiabatic and all other parameters are selected the same as the first case ( $Kn = 0.05$ ).

The below Figure 4.13 shows the pressure and velocity variation on parabolic nose cone surface.



(a) Pressure

Figure 4.13: Pressure distribution (a) comparison between solution of *rhoCentralFoam* with slip BC and CFD results on Parabolic shape solid surface

The below Figure 4.14 shows the pressure and velocity contours on the parabolic nose cone shape.

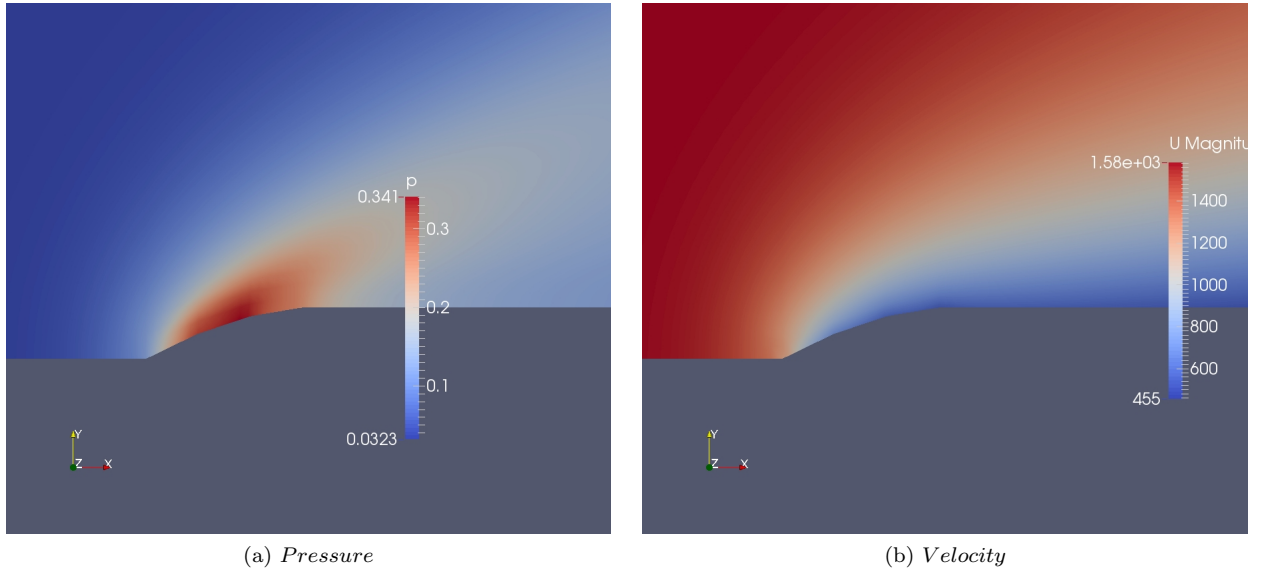


Figure 4.14: Pressure distribution (a) and velocity (b) contours of parabolic nose cone

This Parabolic nose cone shape has min tip pressure.

## Spherically blunted nose cone

The below Figure 4.15 shows Pressure and Velocity distribution on Spherically blunted nose cone.

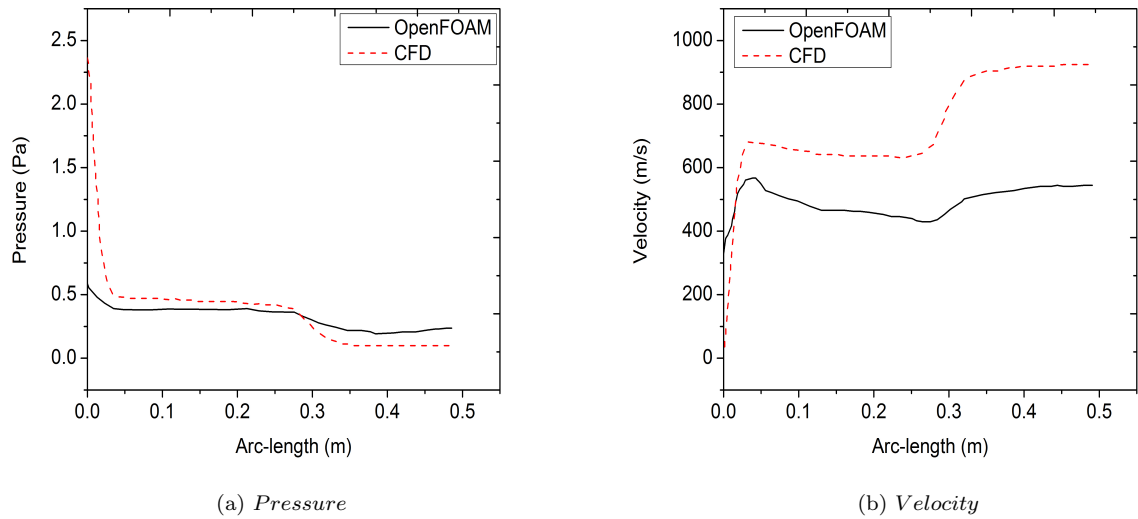


Figure 4.15: Pressure distribution (a) and velocity (b) comparison between solution of *rhoCentralFoam* with slip BC and CFD results on Sp.Blunted shape solid surface

The below Figure 4.16 shows the Pressure and Velocity contours.

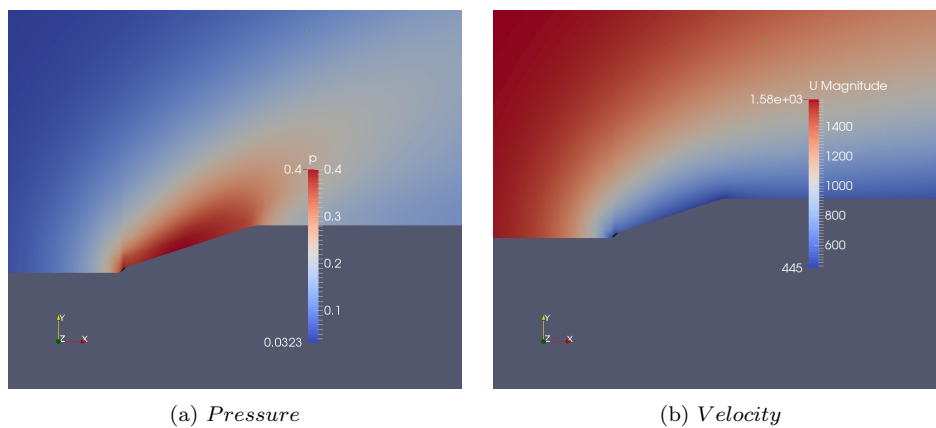
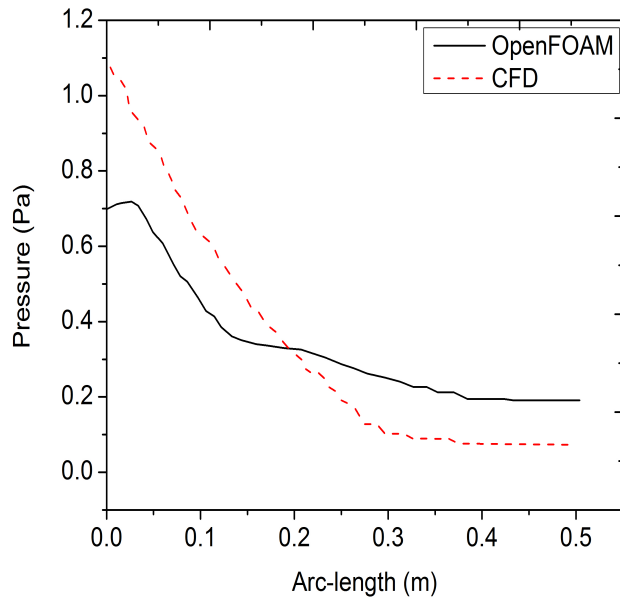


Figure 4.16: Pressure distribution (a) and velocity (b) contours on Spherically blunted cones

### Tangent Ogive nose cone

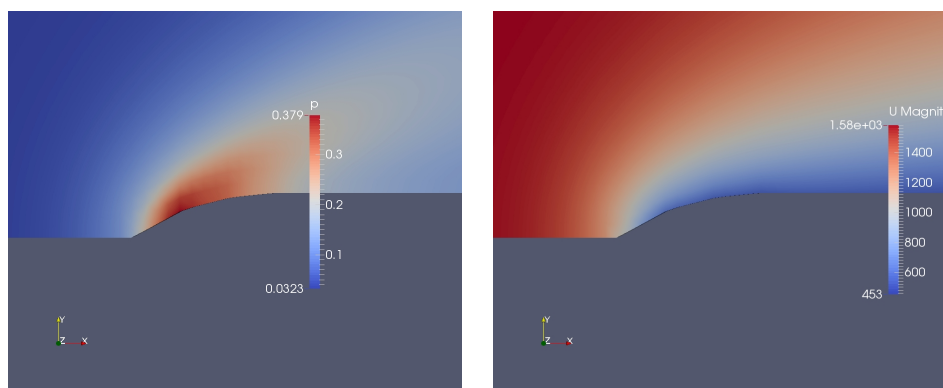
The below Figure 4.17 shows Pressure and Velocity distribution on Spherically blunted nose cone.



(a) Pressure

Figure 4.17: Pressure distribution (a) comparison between solution of *rhoCentralFoam* with slip BC and CFD results on Tangent ogive shape solid surface

The below Figure 4.18 shows the Pressure and Velocity contours.



(a) Pressure

(b) Velocity

Figure 4.18: Pressure distribution (a) and velocity (b) contours on Tangent Ogive cone

### Bi-conical nose cone

The below Figure 4.19 shows Pressure and Velocity distribution on Spherically blunted nose cone.

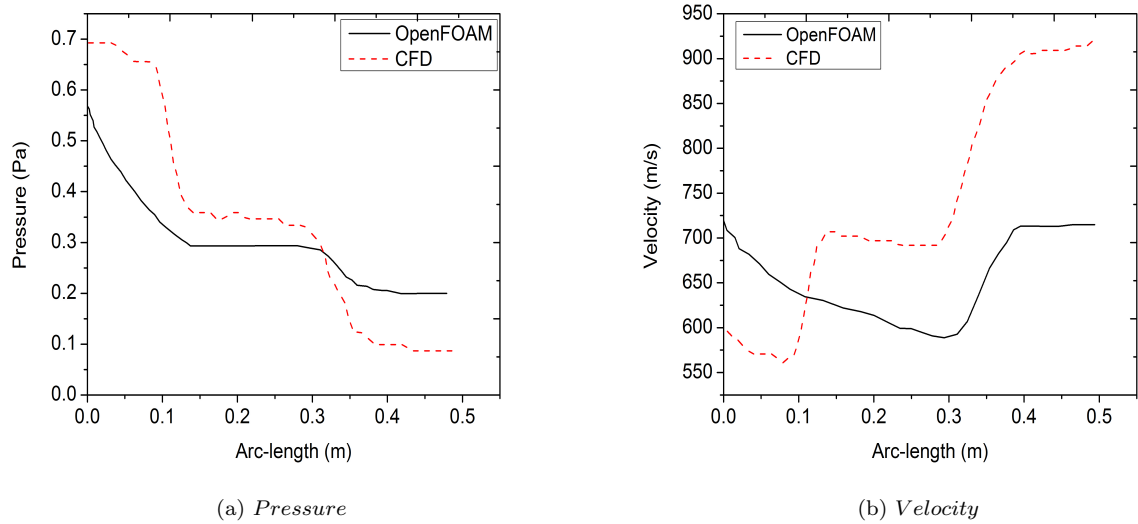


Figure 4.19: Pressure distribution (a) and velocity (b) comparison between solution of *rhoCentralFoam* with slip BC and CFD results on Bi-conical shape solid surface

The below Figure 4.20 shows the Pressure and Velocity contours.

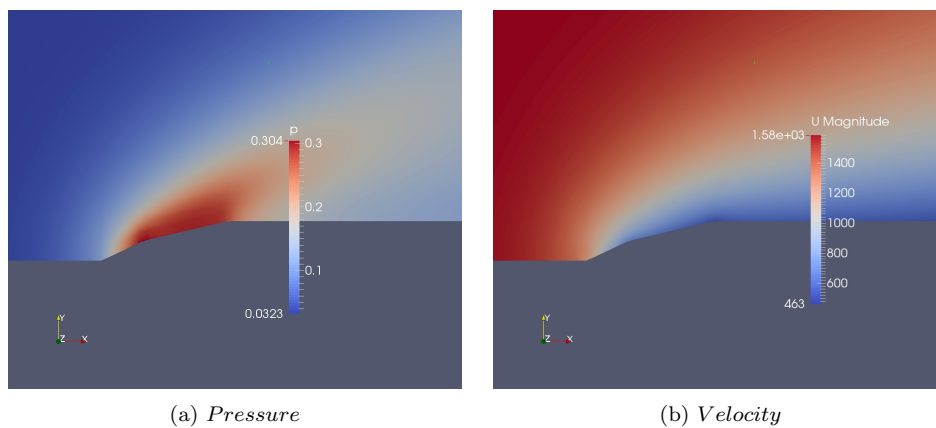


Figure 4.20: Pressure distribution (a) and velocity (b) contours on Bi-conical nose cone

### Conical nose cone

The below Figure 4.21 shows Pressure and Velocity distribution on Spherically blunted nose cone.

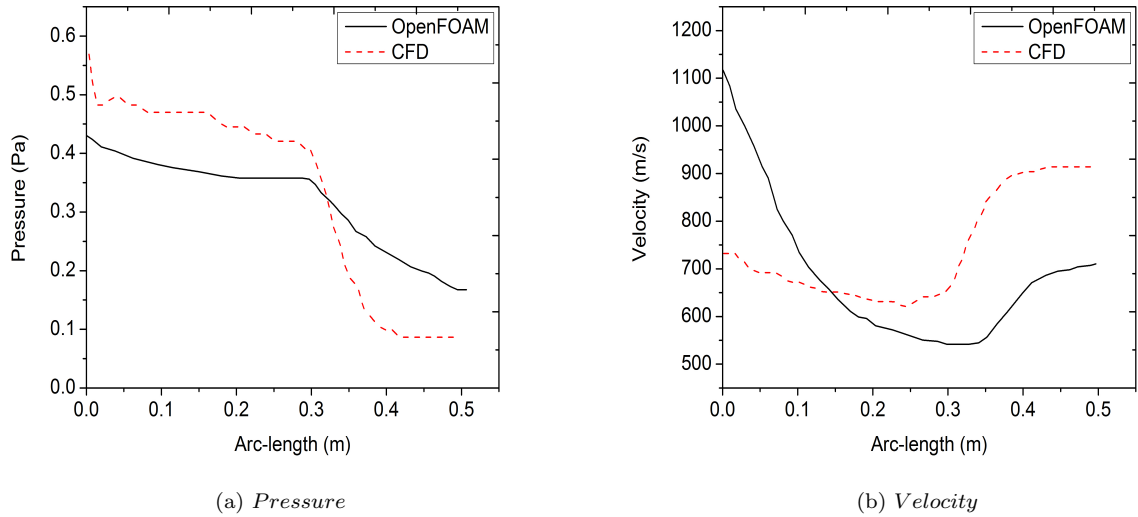


Figure 4.21: Pressure distribution (a) and velocity (b) comparison between solution of *rhoCentralFoam* with slip BC and CFD results on Conical shape solid surface

The below Figure 4.22 shows the Pressure and Velocity contours.

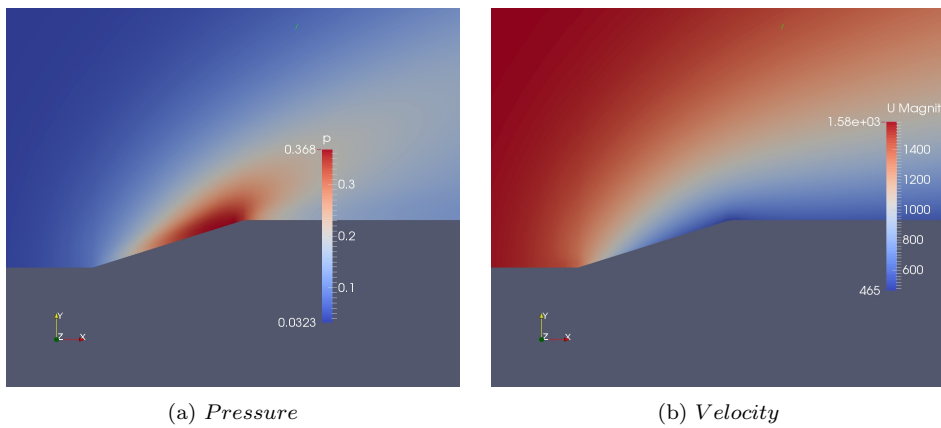


Figure 4.22: Pressure distribution (a) and velocity (b) contours on Conical nose cone



#### 4.4.2 Pressure Distribution Comparison on all nose once shapes

As the Knudsen number is 0.5 in which the flow regime is called as transition flow. In this flow regime the non-equilibrium molecules will be unsteady and to obtain the aero-dynamic parameters would be very difficulty.

At high altitudes the pressure is less in the rarefied regime but which effect the designing factors of missiles and flights. The nose cone should posses less pressure which is desirable for the designing. The below Figure 4.4.2 shows the comparison of Pressure among all the nose cone shapes such as Conical, Bi-conical, Spherically blunted, Parabolic and Tangent ogive shapes. From the above

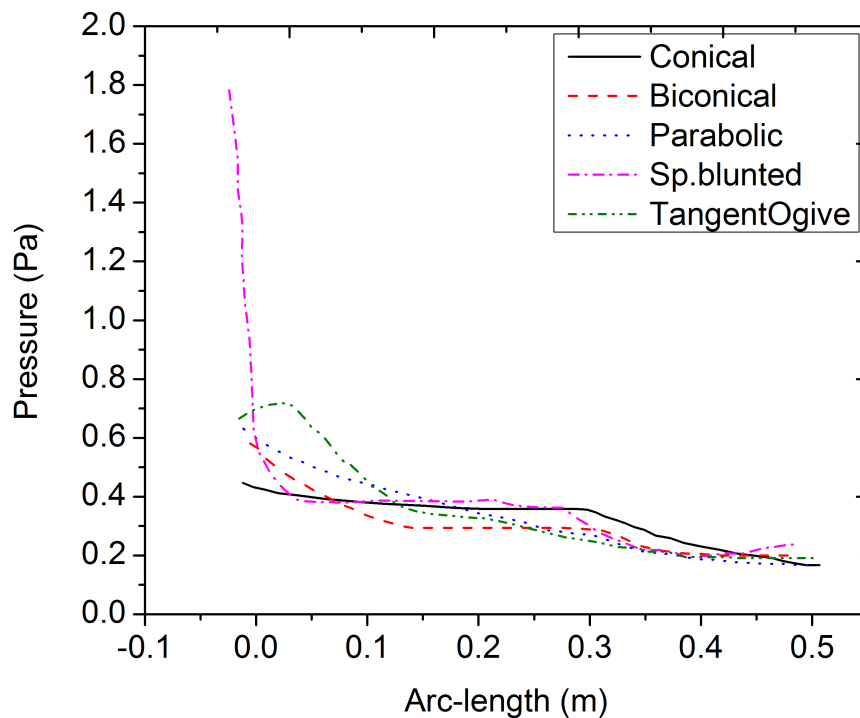


Figure 4.23: Variations in Pressure on various nose cone shapes at  $Kn = 0.5$

graph Spherically blunted cone has maximum tip pressure and also has maximum mean pressure. The minimum tip pressure possessed by Parabolic nose shape and Bi-conical nose shape

### 4.4.3 Wall Shear Stress

Wall shear stress is also one of the most considerable factor while designing the missile/bullet/wing because if the wall shear stress is high gives maximum temperature which leads damage the the missile and carrying things in it. So the nose cone shape also play vital role in the reduction of shear stress on the missile. Whatever shapes give minimum wall shear stress we prefer that shape for the designing of missile. The below Figure 4.4.3 shows the comparison of wall shear stress on each nose cone shapes

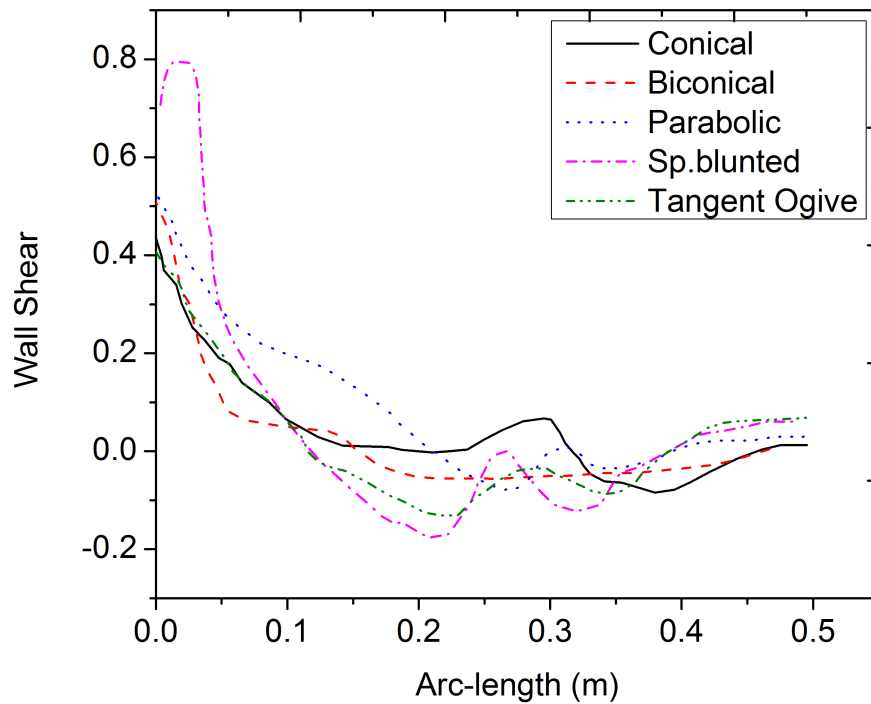


Figure 4.24: Variations in Wall Shear on various nose cone shapes at  $Kn = 0.5$

From the above graph Parabolic nose cone shape and Tangent Ogive nose cone shape have minimum average shear stress. So those two cone shapes are preferable while designing the missile/bullet/wing.

#### 4.4.4 Temperature Variations on all nose cone shapes

Temperature distribution over the missile/bullet/flights should be minimum for not to damage the vehicle and the things which carries inside it. While for re-entry vehicles, the temperature have to be maintained at minimal condition. The nose cone shape is considerable factor to maintain the minimum temperature at tip (nose) and should posses less temperature at desired velocity. The below Figure 4.4.4 shows the all nose cone temperatures.

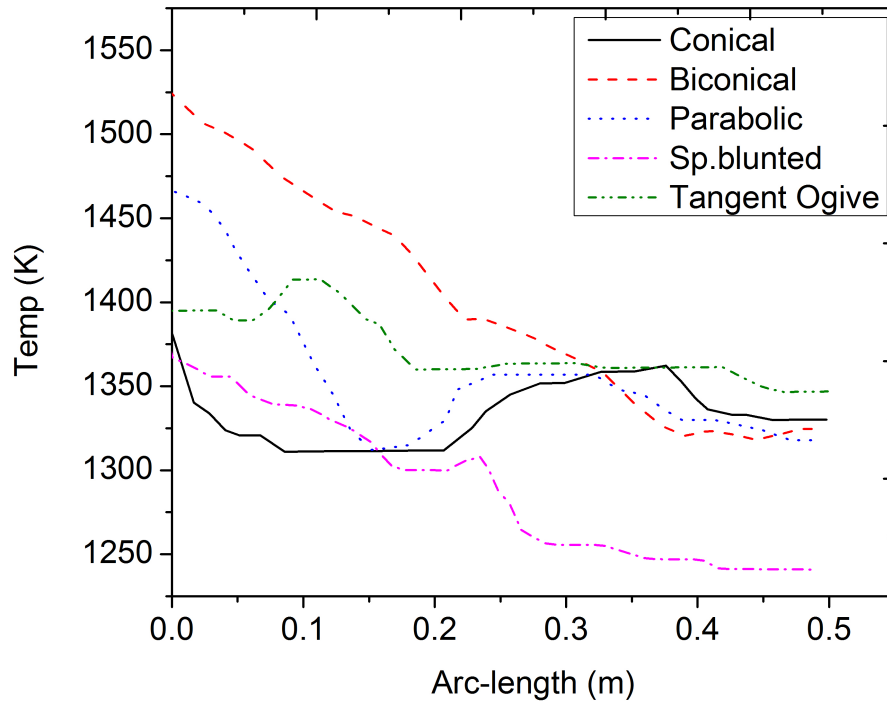


Figure 4.25: Variations in Wall Shear on various nose cone shapes at  $Kn = 0.5$

From the above graph Parabolic shape has minimum tip temperature and Tangent Ogive nose cone shape has minimum mean surface temperature.

#### 4.4.5 Velocity Variations on all nose cone shapes

The missile and flights should not effect with more drag and they have to move desired velocity. If Flight and missile go down below desirable velocity which could effect them.

The below Figure 4.4.5 shows the velocity variation around the solid surface of all nose cone shapes.

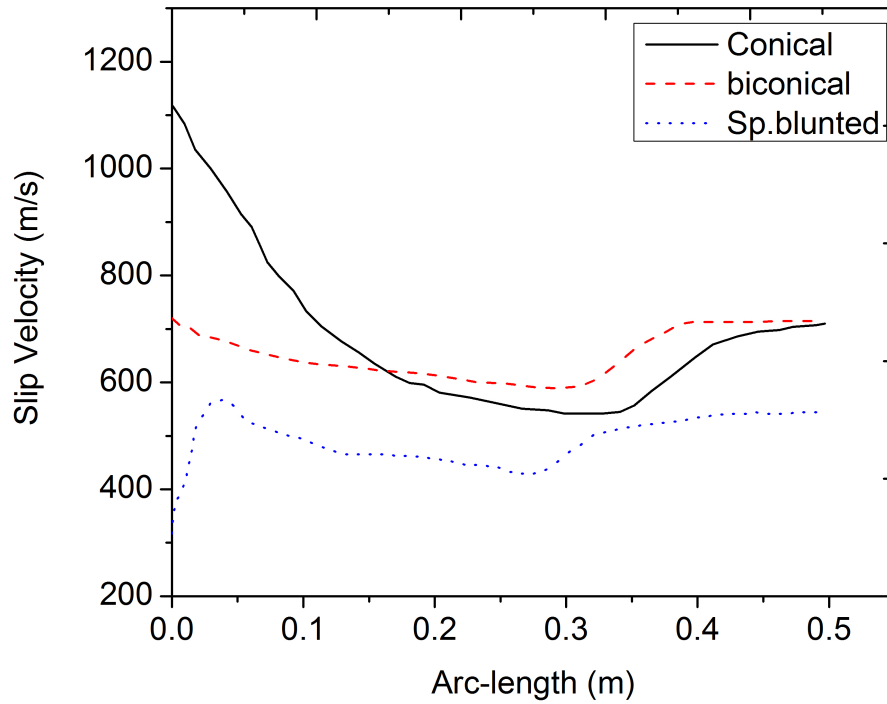


Figure 4.26: Variations in Slip Velocity on various nose cone shapes at  $Kn=0.5$

As flow is transition, it is very difficult to treat the flow properties.

## Chapter 5

# Grid Independence

Grid convergence is the term used to describe the improvement of results by using successively smaller cell sizes for the calculations. A calculation should approach the correct answer as the mesh becomes finer, hence the term grid convergence. In this section we look at the three runs of the same problem but on very different grids. These show how well the software copes with a changing scale and how very close it is to having grid independence.

The Grid Independence test has been imposed on both Conical and Bi-conical nose cone shapes with coarse mesh and finer mesh. The flow parameters such as Pressure coefficient and pressure has tested to know about grid independence. The values have excellent agreement for the grid independence test.

### 5.1 Grid independence test on Conical and Bi-conical nose cone

As we mentioned above we have found the grid independence on Conical and Bi-conical nose cone shapes with different cells.

The below Figure shows the grid independence test on conical nose cone shape with the parameter Pressure Coefficient.

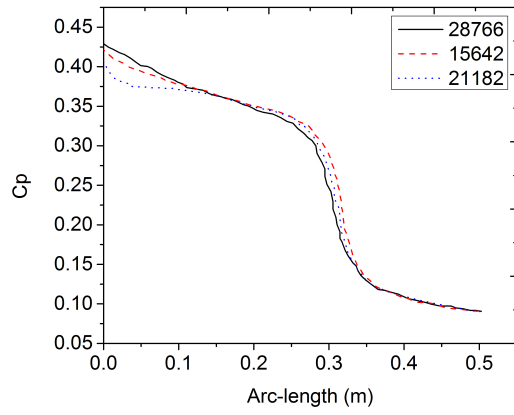


Figure 5.1: Variations in Pressure Coefficient on Conical nose cone

and also, we have found flow parameter pressure for grid independence test with different cells, and given good agreement.

The below Figure shows the grid independence test on conical nose cone shape the flow parameter Pressure.

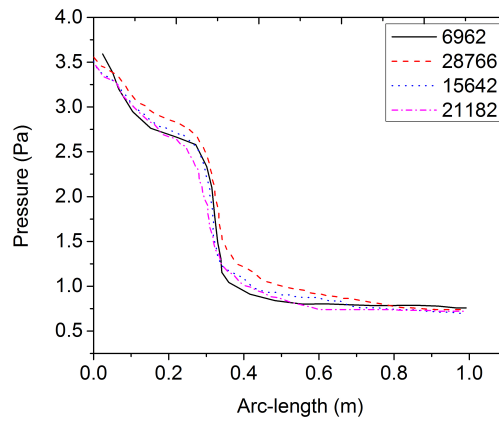


Figure 5.2: Variations in Pressure on Conical nose cone

The below Figure shows the grid independence test on Bi-conical nose cone shape with the parameter Pressure Coefficient.

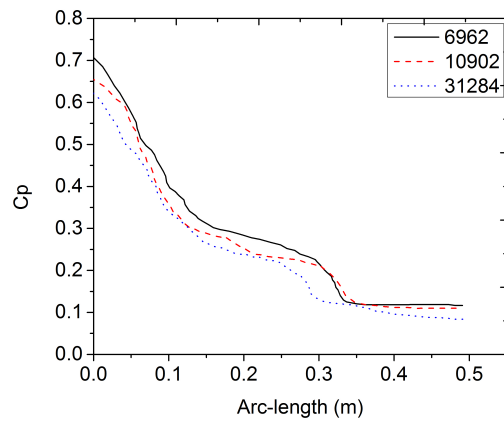


Figure 5.3: Variations in Pressure Coefficient on Bi-Conical nose cone

and also, we have found flow parameter pressure for grid independence test with different cells, and given good agreement.

The below Figure shows the grid independence test on Bi-conical nose cone shape the flow parameter Pressure.

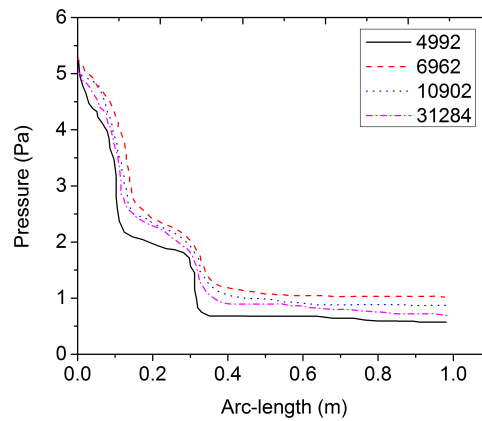


Figure 5.4: Variations in Pressure on Bi-Conical nose cone

## 5.2 Time independence

Time Independence test is keeping the grid fix, and refine the time-step. Since the time-step-size and cell-size are connected via Courant number so that the solution is time-step independent for the current mesh-size. We have performed the time-independence test on Conical nose cone shape by considering the Pressure coefficient as flow parameter. We have increased the end time and took  $C_p$  on each end time plot the graph among them and reasonably got agreement among them. The below Figure shows the time-independence on Conical nose cone shape by considering the pressure coefficient as flow parameter.

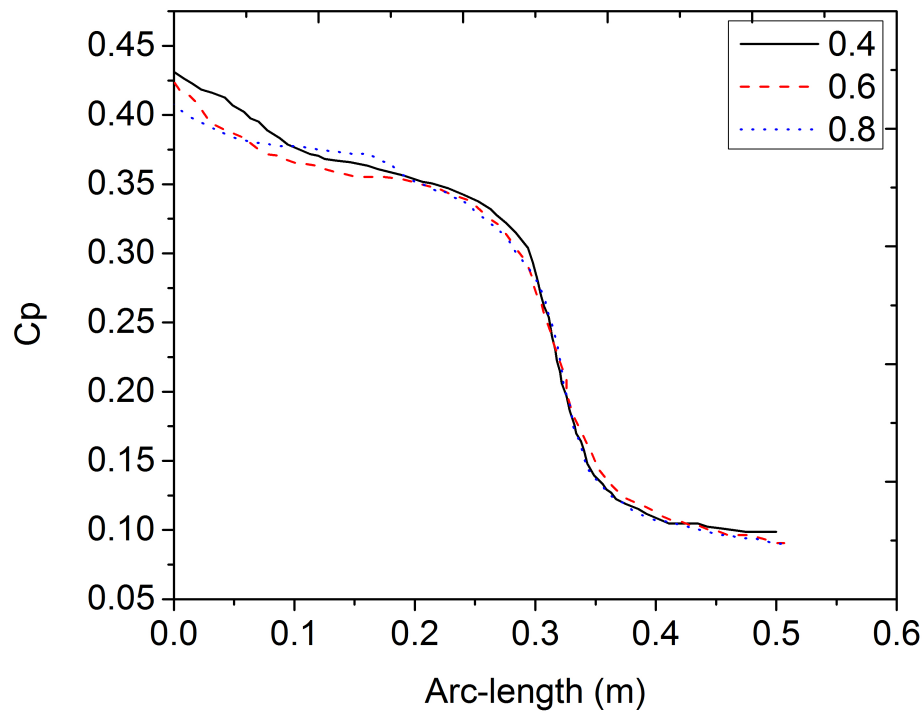


Figure 5.5: Variations in Pressure Coefficient on Conical nose cone

We got reasonably agreement on each end time.



## Chapter 6

# Conclusion and Future work

We have presented aero-dynamics parameters on five critical nose cone shapes such as Conical, Bi-conical, Spherically blunted, Parabolic and Tangent Ogive in rarefied flow. The *rhoCentralFoam* have validated against CFD results. We have carried out detailed investigations to report the non equilibrium effects on the drag and lift coefficients and wall shear stresses.

We have arrived that Parabolic nose cone has minimum mean temperature and pressure. Even Tangent Ogive nose cone shape too reasonably minimum mean surface temperature. So, both nose cone shapes are desirable for the flights, missiles and bullets. As can be seen, the pressure contours are in the excellent agreement but the velocity contours illustrate some differences. the source of this discrepancy is related to the inaccuracy of Maxwell's velocity slip boundary condition. This boundary condition valid for the Knudsen number  $Kn$  between 0.01 and 0.1 and, therefore with increasing Knudsen number  $Kn$  from 0.01, the accuracy of this boundary condition is reduced.

The first-order non-equilibrium boundary conditions are not sufficient to accurately describe the non-equilibrium gas flow physics. We may need to incorporate both the higher order boundary conditions as well as the non-linear constitutive relations into the Navier-Stokes equations framework to report better predictions. This can be done as a future work to this current work. This is very important from the numerical simulations perspective as particle methods are still computationally intensive for simple gas flows and indeed expensive for 3-D complex geometries.

# References

- [1] T. B. J. P. C.J. Roy, M.A. Gallis. Navier-Stokes and DSMC simulations for hypersonic laminar shock-shock interaction flows. *AIAA Paper 2002-0737* .
- [2] R. C. J.J. Bertin. Critical Hypersonic aerodynamic phenomena. *Annu. Rev. Fluid Mech* 38, (2006) 129–157.
- [3] G. P. Wood. Calculations of surface temperatures in steady Supersonic flight. *NACA TN No. 1114* .
- [4] W. Hasse. Solution of the Navier Stokes equations for sub and supersonic flows in rarefied gases. *Numerical fluid Mechanics* 139–157.
- [5] Vieweg and Sohn. Numerical Simulation of Compressible Navier -Stokes Flows. *Numerical fluid Mechanics* 18.
- [6] Z. Wang and L. Bao. Aerothermodynamics of hypersonic small nose cone with local rarefied gas effects. *Chinese Journal of Computational Physics* 27(1), (2010) 59–64.
- [7] M. Gauer. Numerical Investigation of a Spiked Blunt Nose Cone at Hypersonic Speeds. *Spacecraft and Rockets* 45, (2008) 459–471.
- [8] G. C. I. Nompelis. US3D predictions of double-cone and hollow cylinder-flare flows at high enthalpy. *AIAA Paper* 2014–3366.
- [9] E. J. I. N. E.Titov, J. Burt. Implications of slip boundary conditions on surface properties in hypersonic flows. *AIAA Paper* 2012–3307.
- [10] S. C. Traugott. Some Features of Supersonic and Hypersonic flow about Blunted Cones. *Journal of the Aerospace Sciences* 29.
- [11] Owens and R. V. Aerodynamic characteristics of spherically blunted cones at Mach numbers 0.5 to 5.0. *NASA Marshall Space Flight Center; Huntsville, AL, United States* 1–69.
- [12] G. L. Burke. Heat Transfer and Pressure Distributions about Sharp and Blunted Elliptic Cones at Angles of Attack and High Mach Numbers. *AFFDL-TR-64-17* 1–69.
- [13] W. F. Santos and M. Lewis. Shock Wave Structure in a Rarefied Hypersonic Flow on Power Law Shaped Leading Edges. *41st Aerospace Sciences Meeting and Exhibit, AIAA 2003-1134* .
- [14] J. S. Jr and P.A.Newman. Supersonic Flow Past Pointed Bodies. *AIAA Journal* 1019–1021.

- [15] <http://www.openfoam.com> 08.
- [16] B. B. S. and T. J. Barth. A One-Equation Turbulence Transport Model for High Reynolds Number Wall-Bounded Flows. *AIAA 30th Aerospace Sciences Meeting and Exhibit* AIAA-91-0610, (1991) 241–282.
- [17] S. P. R. and A. S. R. A one equation turbulence model for aerodynamic flows. *AIAA 30th Aerospace Sciences Meeting and Exhibit* AIAA 92-0439, (1992) 241–282.
- [18] A. Kurganov, S. Noelle, and G. Petrova. Semidiscrete central-upwind schemes for hyperbolic conservation laws and Hamilton–Jacobi equations. *SIAM Journal on Scientific Computing* 23, (2001) 707–740.
- [19] A. Kurganov and E. Tadmor. New high-resolution central schemes for nonlinear conservation laws and convection–diffusion equations. *Journal of Computational Physics* 160, (2000) 241–282.
- [20] L. G. J. M. R. Christopher J. Greenshields, Henry G. Weller. Implementation of semi-discrete, non-staggered central schemes in a colocated, polyhedral, finite volume framework, for high-speed viscous flows. *INTERNATIONAL JOURNAL FOR NUMERICAL METHODS IN FLUIDS* .
- [21] R. Leveque. Finite Volume Methods for Hyperbolic problems. *1st Edition, Cambridge University Press* .
- [22] e. W.D. Niven. Scientific papers of James Clerk Maxwell. *Dover Publications, Inc.*, 1, p.466.
- [23] W. Sutherland. The viscosity of gases and molecular force. *Philosophical Magazine, S. 5*, 36 507–531.
- [24] M. A. S. E. B. Arkilic and K. S. Breuer. Gaseous slip flow in long microchannels. *Microelectromechanical Systems, Journal of* 6 167–178.
- [25] S. Colin. Rarefaction and compressibility effects on steady and transient gas flows in microchannels. *Microfluidics and Nano fluidics* 1 268–279.
- [26] M. G. el Hak. The fluid mechanics of microdevices the Freeman scholar lecture. *Journal of Fluids Engineering* 121 5–39.
- [27] M. G. el Hak. Molecular gas dynamics and the direct simulation monte carlo of gas flows. *Clarendon, Oxford* 508. .